Influence of temperature cycles on strength and microstructure of spray-deposited Si–Al CE9F alloy

D. Mauduit[a,b], G. Dusserre[a,*], T. Cutard[a]

[a] Institut Clément Ader (ICA), Université de Toulouse, CNRS, IMT Mines Albi, UPS, INSA, ISAE-SUPAERO, Campus Jarlard, 81013 Albi CT Cedex 09, France
[b] CNES, 18 Avenue Edouard Belin, 31400 Toulouse, France

ABSTRACT

This paper investigates the effects of temperature cycles between $-55\,°C$ and $125\,°C$ (the temperature range for intended space application) on the strength and microstructure of spray deposited Si–Al CE9F alloy. After 500 cycles, the strength is significantly improved of 9% (i.e., 26 MPa). Moreover the Weibull modulus also undergoes a significant increase. Microstructure characterizations by XRD, SEM, EBSD and DSC evidence recovery and recrystallization processes in the Al phase, and subgrain development at grain boundaries in the Si phase, leading to lower crystallite size. A Hall–Petch dependence of mean strength to average crystallite size in Si is proposed as strengthening mechanism.

1. Introduction

The usage of spray-deposited Si–Al alloys in space applications mainly encompasses chip boxes aiming at protecting the on-board electronic devices from the environment. Ensuring the tightness of the housing throughout the life cycle of the device is therefore required. In space application, the boxes are subjected to cyclic temperature changes, usually between $-55\,°C$ and $125\,°C$, that may result in structure damage or material properties changes. Therefore, the design of the boxes must take into account the influence of the successive temperature changes on the strength of the material. The present paper thereby focuses on the influence of cyclic temperature changes on the residual strength of a Si–Al CE9F alloy.

Several grades of alloys with various Si–Al ratios (named based on their coefficient of thermal expansion: CE7, CE9, CE11, CE13 and CE17) were recently studied (Weinshanker et al., 2004; Del Castillo et al., 2013). These alloys can be elaborated through several processes (direct metal deposition (Zhao et al., 2014), sintering (Zhai et al., 2014)) or spray-deposited by atomization (Wang et al., 2004). The microstructure (Raju and Ojha, 2014) and the thermo-mechanical properties of the alloy change significantly depending on the processing route. The family of controlled expansion (CE) spray-deposited Si–Al alloys is processed by atomization by Sandvik Osprey™. The major influencing parameters of the atomization process (Cui et al., 2009) (for instance: pressure and temperature during the hot isostatic pressing step to decrease the porosity (Jia et al., 2014; Yu et al., 2012) and gas/

metal mass flow ratio (Wei et al., 2007b)) were evidenced and optimized to obtain the desired specific microstructure and the corresponding material properties. Among these latter, the coefficient of thermal expansion is of prior interest for the intended applications, and several studies (Jia et al., 2014; Hogg et al., 2006) focused on relating it to the specific two-phase microstructure of spray deposited hypereutectic Si–Al alloys.

The present paper deals with the Si–Al grade CE9F, an alloy that contains 60 wt.% silicon and 40 wt.% aluminum. The main characteristics of this material (i.e., a low coefficient of thermal expansion ($9.10^{-6}\,K^{-1}$ between $-20\,°C$ and $100\,°C$), a high thermal conductivity ($130\,W\,m^{-1}\,K^{-1}$) and a low density ($2460\,kg\,m^{-3}$)) make it suitable as chip boxes material for space components. The thermal properties of this alloy are well known, since heat extraction is an important in-use function of the chip boxes. Previous studies (Adolfi et al., 2002; Wei et al., 2007a) evidenced the quasi-linear variation of heat conductivity, heat capacity and diffusivity from room temperature up to 500 °C. Some basic mechanical properties, such as flexural strength and Young's modulus, are also available in literature, but most of the data were measured at room temperature and do not consider preceding temperature cycles.

In a previous paper (Mauduit et al., 2016), the strength of the Si–Al CE9F alloy has proved to be consistent with the Weibull's theory of brittle materials fracture between $-50\,°C$ and $130\,°C$. The fracture surface revealed cleavage mechanisms in the silicon phase. The Weibull's theory is based upon the role of flaws in the strength of brittle

---

materials and accounts for volume effects on the probability of failure (Eq. (1)) (Weibull, 1951; Andreasen, 1994; Trustrum and Jayatilaka, 1977), without requiring any intrinsic feature of the flaws. Eq. (1) expresses the probability of failure, P, of a specimen as a function of stress, σ. m is the Weibull modulus, V_{eq} is the equivalent volume of the sample calculated according to the Weibull's theory, V_0 is a reference volume and σ_0 is the scale parameter.

$$P = 1 - exp\left[-\frac{V_{eq}}{V_0}\left(\frac{\sigma}{\sigma_0}\right)^m\right] \tag{1}$$

As shown in (Mauduit et al., 2016), Weibull's theory accounts for differences between four-point and three-point bending strength of Si–Al CE9F, as a result of volume effects. The Weibull's parameters were found to be independent on temperature between $-50\,°C$ and $130\,°C$, but the material was only subjected to monotonous variation of the temperature and short dwell-times (a few tens of minutes) at $-50\,°C$ or $130\,°C$. In the case of temperature cycles, cyclic stresses are also induced in the material because of the mismatch of coefficient of thermal expansion between aluminum and silicon and may affect the material properties.

The present paper investigates the influence of preceding temperature cycles between $-55\,°C$ and $125\,°C$ on the residual strength at room temperature of the Si–Al CE9F alloy. A significant increase in strength of 9% after 500 cycles is reported for the first time for such a material (to the best of the authors' knowledge). The microstructure of the as-received material is described, and further investigations of microstructure changes after temperature cycles are reported in order to propose a strengthening mechanism.

2. Experiment

The spray deposited Si–Al CE9F alloy was prepared through atomization process by Osprey Metals Ltd (Coombs and Dunstan, 1993). Ninety $45 \times 4 \times 3\,mm^3$ specimens were machined and split into 5 batches intended for different heat treatments. A first reference batch of 29 specimens was used for characterizing the as-received material. Four batches of 10 or 20 specimens were subjected to 80, 200, 500 or 700 temperature cycles performed inside a thermal chamber. The cycles consist of 15 min dwell-times at $-55\,°C$ and $125\,°C$, with heating and cooling rates of $20\,K\,min^{-1}$.

Four-point bending tests were performed at room temperature according to the standard EN-843. The distance between the upper loading points was 20 mm and the distance between the lower supports was 40 mm. The tests were carried out at a constant crosshead displacement rate of $0.5\,mm\,min^{-1}$. Further details about the experiment are available in (Mauduit et al., 2016). All the specimens of each batch were tested. For the batches subjected to 0, 80 and 500 cycles (29, 20 and 20 specimens per batch respectively), the results were analyzed in the framework of the Weibull's theory applied to the fracture of brittle materials (Eq. (1)). For those three batches, the model parameters, σ_0 and m, were identified from the strength values by the maximum likelihood method (Wu et al., 2006; Przybilla et al., 2013).

For each batch, about ten samples were analyzed prior to mechanical test with an X-ray diffractometer (Philips X-PERT) with $Cu\,K\alpha_1$ radiation (wavelength of 0.154184 nm). The incidence angle 2θ ranged between 20° and 130° with a step of 0.0167°. The diffraction lines were analyzed using PANalytical X'Pert High Score software (Degen et al., 2014). A Williamson–Hall analysis (Williamson and Hall, 1953; Pelleg et al., 2005) was conducted both for silicon and aluminum phases in order to assess the changes in crystallite average size and lattice strain after heat treatment through a qualitative analysis of the peak broadening, β, as a function of 2θ. Once removed the instrumental broadening and assuming arbitrarily Cauchy–Lorentz distribution, β is additively decomposed into a size-induced broadening contribution, $\beta_D = \frac{K\lambda}{Dcos\theta}$, and a strain-induced broadening contribution, $\beta_\varepsilon = 4\varepsilon tan\theta$,

leading to the following equation:

$$\beta cos\theta = 4\varepsilon sin\theta + \frac{k\lambda}{D} \tag{2}$$

In Eq. (2), λ is the wavelength of the anticathode and k (the shape parameter of the Scherrer law (Jones, 1938; Stokes and Wilson, 1943)) is set to 1 when integral width is considered. ε and D are respectively deduced from the slope and intercept of a linear fit of $\beta cos\theta$ versus $sin\theta$. It is noteworthy that only qualitative results are obtained through this method (cf. (Scardi et al., 2004) for a critical discussion). However a comparative analysis of the different batches will provide an insight into the mechanisms at work during temperature cycles. In addition, some specimens of the reference batch were subjected to heat treatment at $130\,°C$ and $200\,°C$ for 20, 50 and 125 h (corresponding respectively to the time spent at $125\,°C$ during 80, 200 and 500 cycles) and characterized by the same method.

From these results, the dislocation density, ρ, is calculated as a function of average crystallite size, average lattice strain and Burgers vector magnitude, b, by using Eq. (3) (Williamson and Smallman, 1956; Chowdhury et al., 2010; Kapoor et al., 2004; Uday et al., 2015). For both Al and Si phases, $b = a\sqrt{2}/2$ (Uday et al., 2015; Godet, 2004), with a, the lattice parameter ($a = 0.543$ nm for Si and $a = 0.404$ nm for Al). K is a material constant that depends on crystallite shape and is generally close to unity (Balzar, 1993).

$$\rho = 2\sqrt{3}\,\sqrt{K}\,\frac{\varepsilon}{D.\,b} \tag{3}$$

The $sin^2\psi$ method, developed by Macherauch and Muller (Macherauch and Muller, 1961), was used to assess the residual stresses in several samples of each batch after heat treatment. In a DRX experiment, the difference of Bragg angle between stressed and unstressed material, $\Delta\theta_{hkl}$, can be related to the lattice strain of the planes of {hkl} type, $\varepsilon_{hkl}^{\phi\psi}$ (Eq. (4)).

$$\varepsilon_{hkl}^{\phi\psi} = -\frac{1}{2}cotan(\theta_{hkl})*\Delta 2\theta_{hkl} \tag{4}$$

The difference of Bragg angle $\Delta\theta_{hkl}$ of the planes of {hkl} type is both function of angles ψ and φ, parameters of the direction of the incident beam at the sample surface. φ is set to 0° in the experiment, and the normal stress is neglected (plane-stress at the surface of the sample), leading to a simplified $sin^2\psi$ law, Eq. (5). The method likewise assumes that the material is homogeneous, isotropic, and that the residual stresses are uniform. Due to the heterogeneity of the material only a comparative analysis of the results will be carried out.

$$\varepsilon_{hkl}^{\phi\psi} = \frac{1}{2}S_{2,hkl}\sigma_{11}sin^2\psi + \frac{1}{2}S_{2,hkl}\sigma_{13}\sin(2\psi) + S_{1,hkl}(\sigma_{11} + \sigma_{22}) \tag{5}$$

In Eq. (5), $S_{1,\,hkl}$ and $S_{2,\,hkl}$ are the radioelastic constants of the planes of {hkl} type and σ_{ij} are the components of the residual stress tensor. Planes of {222} type in the Al phase (theoretical Bragg angle of 156.7°) were analyzed with chromium radiation (wavelength of 0.2085 nm). Assuming that $\sigma_{11} = \sigma_{22}$, an elliptical fit of $\varepsilon_{hkl}^{\phi\psi}$ versus $sin^2\psi$ provides the value of the components of the stress tensor $\sigma_{11} = \sigma_{22}$ and σ_{13}. The former quantity will be referred to as the residual stress.

The microstructure of the material was characterized by Electron Backscattered Diffraction (EBSD HKL system), with a Scanning Electron Microscope (SEM) JSM-7100TTLS LV. A $50 \times 50\,\mu m^2$ area of one as-received specimen was prepared by Focused Ion Beam (FIB) to characterize the reference material microstructure. The microstructures of the reference material and of a sample subjected to 500 temperature cycles were compared on a larger area ($200 \times 150\,\mu m^2$) prepared by standard mechanical polishing.

Differential Scanning Calorimetry (DSC) experiments were performed using a Perkin Elmer DSC8500 apparatus. Two samples of about 15 mg taken from a reference specimen (as-received) and from a specimen previously subjected to 500 temperature cycles, were heated from 50 up to $500\,°C$ at $20\,K\,min^{-1}$ under N_2 flow.
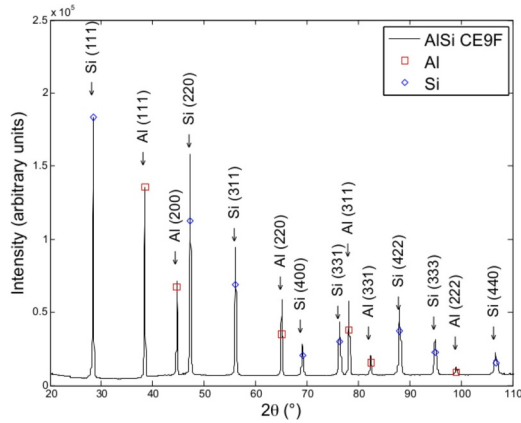
Fig. 1. Diffraction pattern of Si-Al CE9F compared to the diffraction peaks of pure Si and Al (the intensity of Si and Al peaks are normalized in reference to the intensity of the first corresponding peak in Si–Al CE9F line) (preference for color: online only).

3. Results

3.1. Microstructure of the as-received material

The microstructure of the as-received material consists of two interpenetrating phases of almost pure Si (diamond cubic) and Al (face-centered cubic). Indeed, the position of the XRD peaks (Fig. 1) matches the data for either pure Si or pure Al (standard JCPDS cards No. 00-005-0565 and 00-004-0787, respectively). Moreover, a comparison of the relative peak intensity for each phase indicates that the grains are macroscopically equiaxed in both phases. The two-phase microstructure resulting from spray-deposition is shown in Fig. 2, where the silicon phase is in light gray and the aluminum phase in dark gray.

A quantitative analysis of 60 optical microscope pictures (× 1000 magnification) taken in three perpendicular planes has shown that the material composition can be homogenized in a 200 μm edge cube (the composition assessed by image analysis is 59.74 ± 0.35 wt.% Si and 40.26 ± 0.35 wt.% Al). Moreover, from this analysis, the microstructure seems isotropic at this level.

EBSD analyses of 200 × 150 μm² areas provide an average grain diameter of 2.5 μm in the Si phase and of 5 μm in the Al phase. The distribution of Si grain diameter is quasi-uniform between 0.5 and 3 μm and includes a few grains up to 10 μm diameter. In the Al phase, the
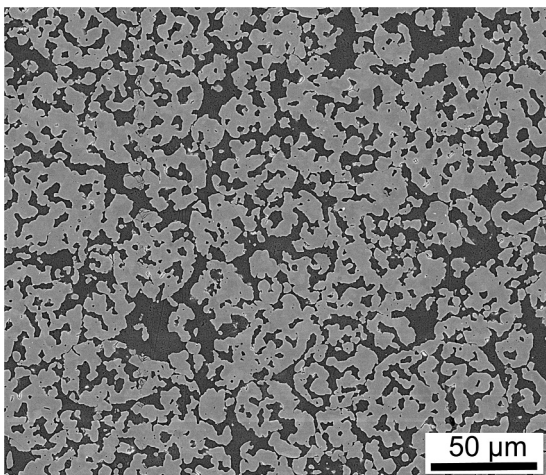

Fig. 2. Two-phase microstructure of Si-Al CE9F alloy (Si in light gray and Al in dark gray). SEM picture using back-scattered electron detector. The sample was mechanically polished following standard procedure and chemically etched with Keller's reagent.

distribution is scattered with a lot of 2 μm diameter grains and several large grains of diameter up to 15 μm. It seems that the Al grain size is directly related to the gap available between the Si grains (Fig. 3).

EBSD analysis of FIB polished surface (50 × 50 μm² areas, Fig. 3) reveals low local misorientation inside the grains (i.e., lower than 0.5° (Mohtadi-Bonab et al., 2015) except in the vicinity of a subgrain boundary) irrespective of the phase considered.

The analysis of the misorientation at the grain boundaries in both Al (Fig. 3c) and Si (Fig. 3d) phases shows some subgrain boundaries with misorientation lower than 5°. The Si phase is characterized by the presence of coherent Σ3 60°/<111> twin boundaries in almost each grain (Fig. 3d). This kind of twin boundaries has a low surface energy (0.06 J m^{-2}) (Phillpot and Wolf, 1990; Bristowe, 1998; Kohyama et al., 1986).

Fig. 4a and b display IPF EBSD maps of large areas (200 × 150 μm²) in Al and Si for a sample mechanically polished. These results confirm that the Si phase is highly equiaxed at this scale. The Al phase seems to exhibit large areas of a few tens of μm with similar crystallographic orientation (cf. the green area at the bottom right of Fig. 4a, and the pink area at the top right of Fig. 3a) even if the grains are not in contact in the image plane, and areas of fine equiaxed microstructure (at the left of Fig. 3a or at the center of Fig. 4a). Such features were already evidenced in the microstructure of Si-Al CE7F by Hogg et al. (2006).

3.2. Effect of temperature cycles

3.2.1. EBSD data

Fig. 4c and d display IPF EBSD map of large areas (200 × 150 μm²) in Al and Si for a sample mechanically polished after exposure to 500 temperature cycles between −55 °C and 125 °C. The microstructure of the sample subjected to 500 temperature cycles is similar to the one of the as-received material in terms of grain size and crystallographic orientation. No quantitative comparison was possible with the available data concerning the fraction of subgrain boundaries in Al, the fraction of twin boundaries in Si, and local misorientation in both phases. However, the histogram of misorientation between two adjacent grains indicates that the number of subgrain boundaries in Si (misorientation lower than 5°) is about twice in Fig. 4d (after 500 cycles) than in Fig. 4b (as-received).

3.2.2. Strength

The mean four-point bending strength for each batch is plotted in Fig. 5 versus the number of temperature cycles. A significant increase of 9%, from 283 MPa up to 309 MPa, is evidenced between 0 and 500 cycles. The trend of the curve is not linear: an increase of 5% is already achieved after 80 cycles. Between 500 and 700 cycles, no significant change is evidenced, which indicates that the phenomena leading to strength increase do not occur any more after such numbers of temperature cycles.

Table 1 reports mean, minimum and maximum values of the strength for each batch, as well as the Weibull parameters for 0, 80 and 500 cycles, for which at least 20 values are available, allowing a proper identification (Nohut, 2014). During the first 80 cycles, mean, minimum and maximum values increase in the same way, as well as σ_0, whereas the Weibull modulus remains unchanged. Between 80 and 500 cycles, the increase in average strength is still significant, but the maximum value and scale parameter only slightly increase, and the minimum value does not change anymore. Moreover the Weibull modulus significantly increases, indicating that the strength distribution is narrower.

The experimental strength distributions after 0, 80, 200, 500 and 700 cycles are plotted in Fig. 6, as well as the identified Weibull curves for 0, 80 and 500 cycles. The shift toward higher values of the Weibull curve illustrates the increase in strength with the number of temperature cycles.
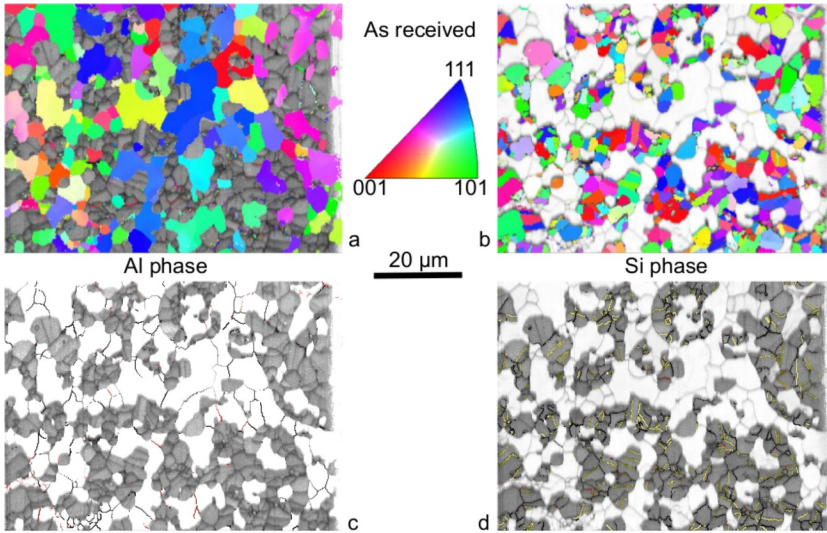
Fig. 3. IPF EBSD maps with respect to the *Z* direction (a and b) and substructures (c and d) of the Al phase (a and c) and the Si phase (b and d). In c and d, red lines depict subgrain boundaries (misorientation <5°) and yellow lines depict twin boundaries (60° misorientation). The sample was polished by FIB. (preference for color: online only).
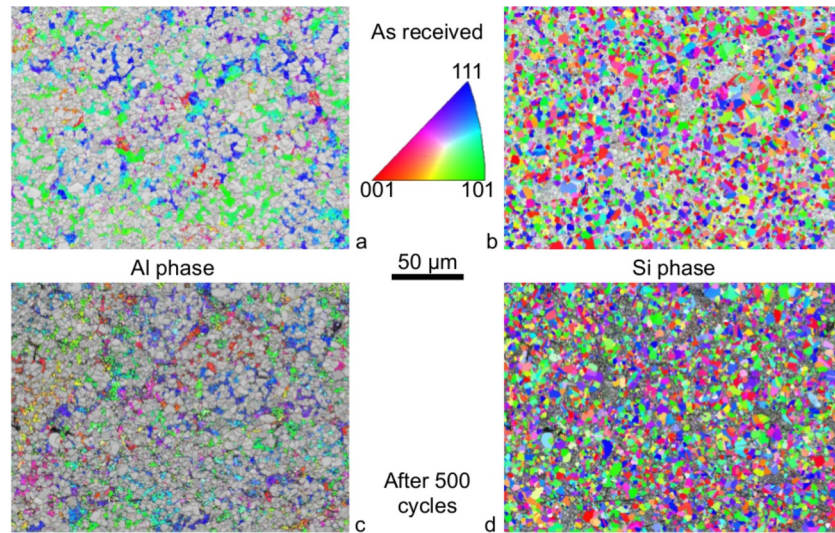

Fig. 4. IPF EBSD maps with respect to the *Z* direction in the Al phase (a and c) and the Si phase (b and d), as received (a and b) and after 500 temperature cycles (c and d). The sample was mechanically polished following standard procedure. (preference for color: online only).

3.2.3. Residual stresses

The assessment of residual stresses in the Al phase by $sin^2\psi$ method provides compressive normal stress values about 20 ± 5 MPa and shear stress values of 5 ± 2 MPa for 0, 200, 500 and 700 temperature cycles and does not evidence any significant change in the residual stress level with the number of temperature cycles. It is noteworthy that the residual stress value is of the order of magnitude of the yield stress of pure aluminum (between 10 and 20 MPa for purity of 99.99 and 99.8% respectively (Davis, 1993)), which indicates that the Al phase has probably undergone plasticity mechanisms during the elaboration of the material.

3.2.4. Williamson–Hall analysis

The Williamson–Hall analysis of the XRD spectra provides an assessment of the average crystallite size and the average lattice strain from Eq. (2), and therefore the dislocation density from Eq. (3), in both Al and Si phases. These data are plotted respectively in Fig. 7a, c and e versus the number of temperature cycles. For comparison purpose, the same data are plotted in Fig. 7b, d and f for samples subjected to heat treatment at 130 °C for 20, 50 and 125 h. These heat treatments correspond to the time spent at the maximal temperature during 80, 200 and 500 cycles respectively. The results obtained with heat treatments at 200 °C are identical to those obtained after heat treatments at 130 °C and are not reported here.

The average crystallite size in the Si phase decreases of about 30% during the first 200 cycles and seems to stabilize after 500 cycles with a total decrease close to 35% (Fig. 7a). On the other hand, it seems to stabilize after only 20 h at 130 °C, with a total decrease close to 25% (Fig. 7b). In the Al phase, the average crystallite size continuously increases with the number of temperature cycles, and achieves an increase of 90% after 700 cycles (Fig. 7a). Heat treatments at 130 °C lead to an increase of only 65% after 20 h and a stabilization afterwards (Fig. 7b). It is noteworthy that the average crystallite size in both phases is more than one order of magnitude lower than the grain size assessed in Section 3.1.

The lattice strain in Si phase strongly decreases of about 30% after 200 temperature cycles and then more slightly to achieve a decrease of 44% after 700 temperature cycles (Fig. 7c). Heat treatment at 130 °C implies a decrease of 29% after 20 h, but the lattice strain does not change anymore afterwards (Fig. 7d). In the same way, the lattice strain in the Al phase decreases of about 38% after 200 temperature cycles and 50% after 700 temperature cycles (Fig. 7c), but remains quite constant during heat treatment at 130 °C (Fig. 7d) after a very low decrease for the first 50 h.
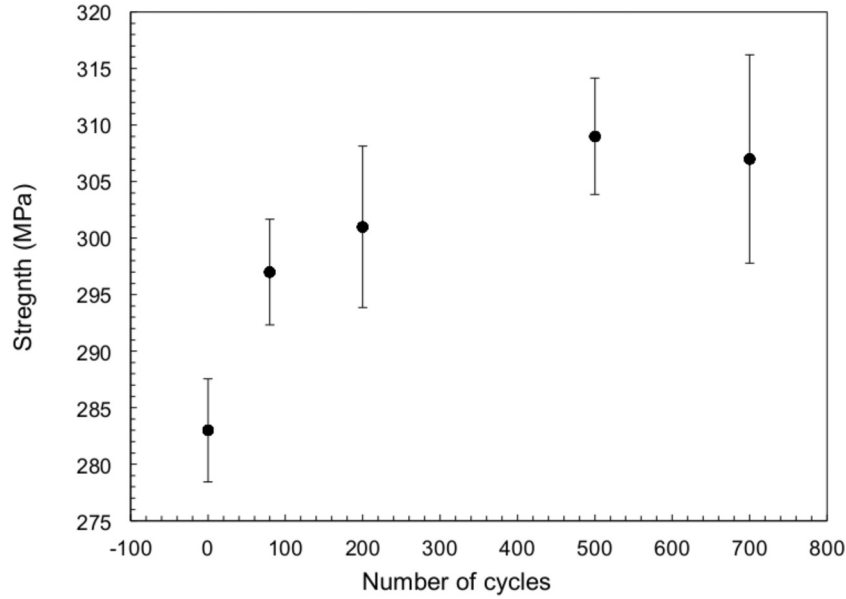
Fig. 5. Increase in mean strength with the number of temperature cycles. The errors bars represent the 95% confidence interval.

The dislocation density in the Si phase, assessed from the previous data using Eq. (3), does not undergo any significant change either during temperature cycling (Fig. 7e) or during heat treatment at 130 °C (Fig. 7f). On the other hand, in the Al phase, the dislocation density exponentially decreases with the number of cycles, with a decrease of 40% after 80 temperature cycles and 74% after 700 temperature cycles (Fig. 7e). After 20 h at 130 °C, the dislocation density has dropped of 50% and does not undergo any change afterwards (Fig. 7f).

3.3. DSC analyses

Fig. 8 compares the DSC thermograms obtained with the as-received material and with a sample previously subjected to 500 temperature cycles. Whereas no significant signal is noticeable for the sample subjected to 500 cycles, the as-received material exhibit two exothermic phenomena. The first one is spread around 150–200 °C and is of low magnitude and the second one is more sharp and manifests as a peak above 400 °C.

Similar results were reported for a strain hardened (H19) commercial 1XXX series alloy in (Hildebrandt, 1979). The low temperature signal consists of several overlapped peaks and is attributed to recovery processes. The high temperature peak is attributed to recrystallization. Recovery peaks were also reported for a recycled aluminum alloy subjected to severe plastic deformation by equal channel angular pressing between 90 and 200 °C (attributed to recovery), between 200 and 300 °C (attributed to recrystallization) and between 300 and 350 °C (attributed to grain growth) (Rebhi et al., 2011; Makhlouf et al., 2012).

The results of Fig. 8 thus indicate that not only recovery processes, but also recrystallization may have occurred in the Al phase during the 500 temperature cycles since the high temperature peak is not present after 500 cycles. The enthalpy corresponding to the first recovery peak between 125 and 250 °C is about 0.03 J g^{-1} (assuming a nominal composition of 40 wt.% Al in the DSC sample). This value lies in the range reported in (Rebhi et al., 2011), between 0.01 and 0.06 J g^{-1}.

4. Discussion

4.1. Microstructural changes in the Al phase

Compressive residual stresses of about 20 ± 5 MPa have been assessed in the Al phase irrespective of the number of temperature cycles. This value is close to the yield stress of pure aluminum (Hildebrandt, 1979) and indicates that the Al phase has probably undergone plastic deformation during the elaboration process. This is supported by the dislocation density about 10^{14} m^{-2} in the Al phase (as-received material). The compressive state of stress in Al probably develops during hot isostatic pressing, because the coefficient of thermal expansion of Al is higher than the one of Si (23×10^{-6} K^{-1} for Al and 2.5×10^{-6} K^{-1} for Si at 25 °C), what would lead to tensile stresses in Al phase during cooling down to room temperature.

The identical results obtained by Williamson-Hall analyses after heat treatments at 130 and 200 °C indicate that the static recovery phenomena are similar in this temperature range and that they are complete after 20 h at 130 °C and a fortiori at 200 °C. These recovery phenomena are probably related to the first DSC peak spread between 125 and 250 °C while scanning at 20 K min^{-1} (Fig. 8), and attributed to recovery in (Rebhi et al., 2011; Makhlouf et al., 2012).

These static recovery phenomena manifest by a large increase of the average crystallite size and a large decrease of dislocation density, but only a low decrease of the lattice strain.

Thanks to cyclic thermomechanical stresses induced by the mismatch of coefficients of thermal expansion, temperature cycles are able to activate dynamic recovery mechanisms that continue the static recovery process. This results in further reducing lattice strain and

Table 1
Strength distribution data as a function of number of temperature cycles.

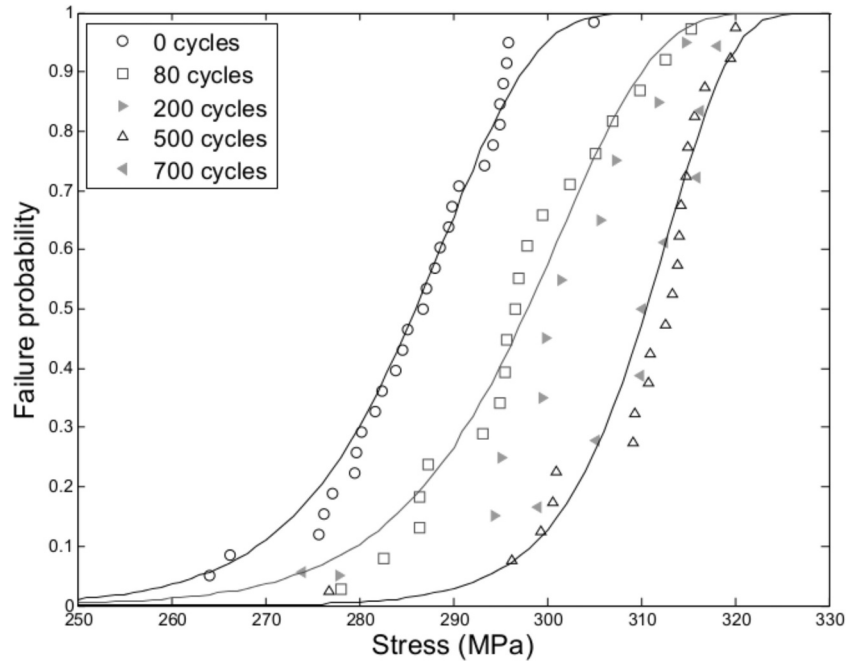| Number of temperature cycles, N	–	0	80	200	500	700
Number of samples, n	–	29	20	10	20	10
Mean value, Rm (std-dev)	MPa	283 (12)	297 (10)	301 (10)	309 (11)	307 (12)
Minimum value	MPa	255	277	278	276	274
Maximum value	MPa	303	315	315	320	318
Weibull modulus, m	–	31	30	–	46	–
Scale parameter, σ_0	MPa	302	316	–	320	–

Fig. 6. Cumulative strength distribution for each batch (markers) and Weibull model identified at 0, 80 and 500 temperature cycles (solid lines). The failure probability estimator for the ith of n values sorted into ascending strength order is $(i-0.5)/n$.

dislocation density and by increasing the average crystallite size. The DSC thermograms indicate that the phenomena occurring during temperature cycles, involve mechanisms related to recrystallization since the high temperature peak (above 400 °C) related to recrystallization (Hildebrandt, 1979) has almost fully disappeared after 500 temperature cycles (Fig. 8). It is noteworthy that recrystallization in super-purity aluminum has been reported at temperature as low as 200 °C (Perryman, 1954) or 250 °C (Huang and Humphreys, 1999).

These static and dynamic recovery phenomena seem to interact during temperature cycles as suggested by the different microstructures obtained after 80 temperature cycles and after 20 h at 130 °C. Indeed, the increase in the average crystallite size is lower and the decrease in lattice strain is higher, after 80 temperature cycles than after 20 h at 130 °C, despite exposure to cyclic thermomechanical stresses in addition to equivalent thermal exposure. However after 200 cycles and 50 h at 130 °C, the microstructural features obtained by Williamson–Hall analysis are about the same and correspond to the stabilized state after heat treatment at 130 °C or 200 °C, which should indicate that the static recovery mechanisms are over. The additional microstructure changes occurring after more than 200 cycles are therefore mainly dynamic and involve recrystallization phenomena.

4.2. Microstructural changes in the Si phase

In the investigated temperature range, dislocation motion in Si is much more difficult (Priester, 2006) than in Al and is not relevant to explain the changes revealed by Williamson–Hall analyses, as confirmed by the almost constant dislocation density provided by Eq. (3) (Fig. 7e and d). However the fraction of subgrain boundaries (misorientation lower than 5°) is about twice after 500 temperature cycles than in the as-received material (cf. Section 3.2.1), and this result is corroborated by the decrease in average crystallite size.

The rapid cooling of the droplets of molten Si during spray forming might have generated crystal defects such as dislocations, twins, but also vacancies and disordered or ill-defined grain boundaries. These latter defects are likely to reorganize and create subgrains with well-defined boundaries instead of ill-defined grain boundaries. Such a phenomenon is consistent with the microstructural changes reported here, i.e., increase in the fraction of subgrain boundaries and decrease of both average crystallite size and lattice strain.

The characteristics of Al and Si phase microstructure follow close trends (i.e., identical results obtained by Williamson–Hall analyses during heat treatments at 130 and 200 °C, slow down of microstructural changes after 200 temperature cycles, and similar values of average crystallite size and lattice strain after either 80–200 cycles or heat treatment for 20–50 h). Together with the previous assumption that changes in Si phase is mainly related to grain boundaries, this could indicate that the interfaces between Al and Si phases are, at least partially, the locus of microscopic changes in Si.

4.3. Strength versus microstructure relationships

The average strength of the material undergoes an important increase up to 80–200 cycles, and then still increases slowly up to 500–700 cycles. Such a two-step trend matches the microstructure changes in the Al and Si phases, as described in Sections 4.1 and 4.2.

However, the strength value, about an order of magnitude higher than the yield stress of pure aluminum (Davis, 1993), and the brittle behavior of the material (Mauduit et al., 2016) indicate that CE9F fracture is mainly related to the Si phase. Indeed, the temperature of brittle to ductile transition in Si is above 500 °C (Hirsch and Roberts, 1991).

The main fracture mechanism in silicon is cleavage along {111} planes (Savage et al., 1993). Evidences of such a fracture mechanism in Si-Al CE9F alloy have been reported in Mauduit et al. (2016) (cleavage planes in fracture surfaces). It is well known from the early work of Petch (1953) that the Hall–Petch effect is relevant to describe the grain-boundary strengthening of materials undergoing brittle fracture by cleavage. Even if the grain size assessed by EBSD does not change with temperature cycles, the strengthening can be related to the decrease of the crystallites size evidenced by the Williamson-Hall analyses. Indeed the subgrain size is sometimes the quantity that controls the mechanical properties instead of the grain size (Ghassemali et al., 2015; McQueen and Hockett, 1970). The plot of average strength as a function of average crystallite size (Fig. 9) shows a reasonable agreement of the experimental data with the Hall-Petch law, in view of the dispersion of the results.
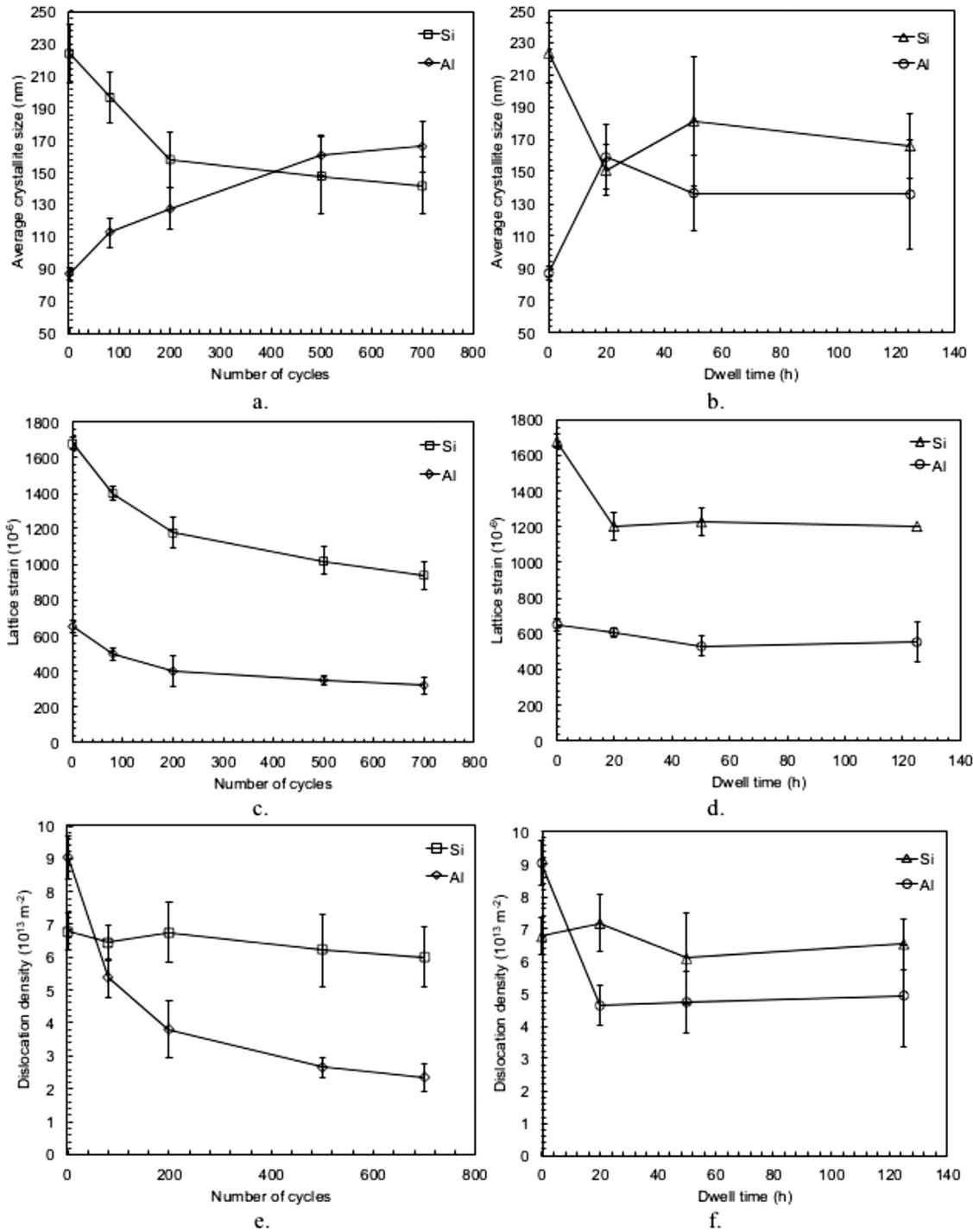
Fig. 7. Evolutions of the average crystallite size (a and b), lattice strain (c and d) and density of dislocations (e and f) in Si and Al phases as a function of temperature cycles number (a, c and e) and of heat treatment duration at 130 °C (b, d and f). The error bars represent the 95% confidence interval. A dwell time of 20, 50 and 125 h respectively corresponds to the exposure time at the maximal temperature for 80, 200 and 500 cycles.

5. Conclusion

Temperature cycles between −55 and 125 °C (in-use temperature range of space embedded systems) induce significant changes in the microstructure and strength of the Si-Al CE9F alloy prepared by spray-deposition.

Recovery and recrystallization occur in the Al phase with a large decrease of the dislocation density. Rearrangement at the grain boundaries (and probably at the interfaces between Al and Si phases, in view of the simultaneous microstructure changes in both phases)

occurs in the Si phase, which leads to a decrease in the average crystallite size.

By Hall-Petch effect, the Si substructure refinement gives rise to an improvement of up to 9% of the strength after 500 cycles, and a lower dispersion of strength values.

Most of these microstructure changes mainly occur between 80 and 200 temperature cycles, and are also observed after heat treatment at 130 °C for 20 h. However, microstructure changes are higher after 500 temperature cycles than after heat treatment. This highlights the role, in the mechanisms a work, of the thermomechanical stresses, induced
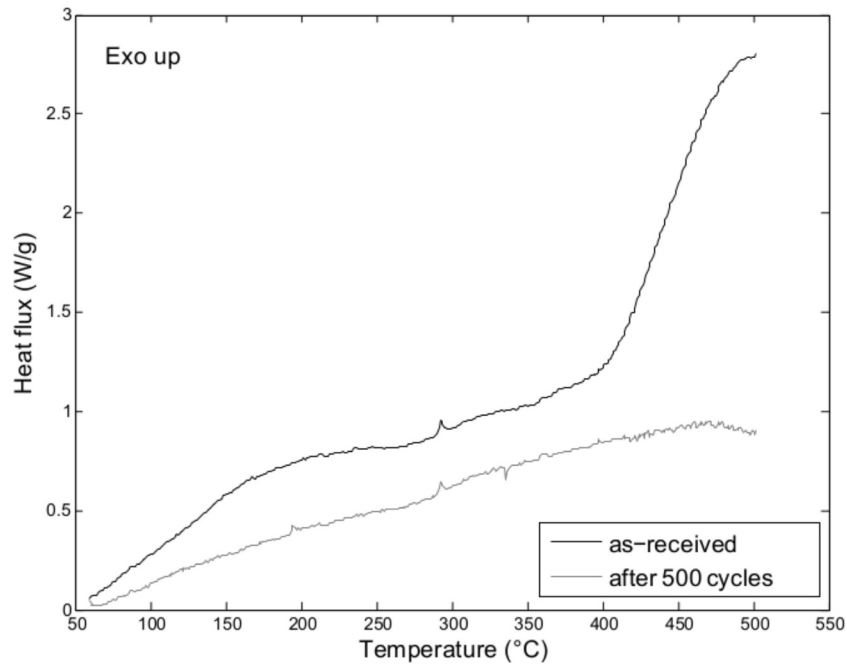
Fig. 8. DSC Thermograms of as-received material and after 500 temperature cycles at 20 K min^{-1}.
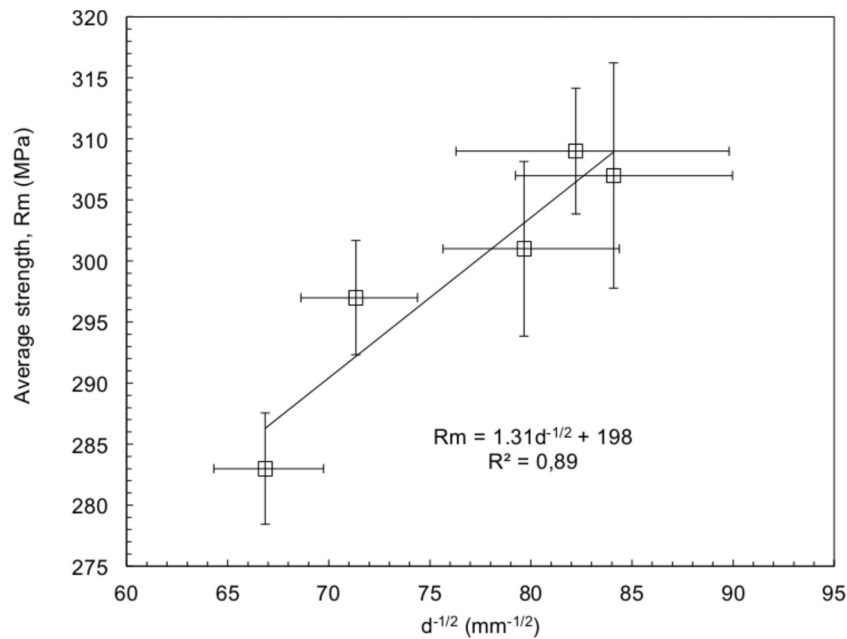

$$Rm = 1.31d^{-1/2} + 198$$
$$R^2 = 0,89$$

Fig. 9. Hall–Petch plot of average strength of Si–Al CE9F, *Rm*, as a function of the Si average crystallite size, *d.* The errors bars represent the 95% confidence interval.

by the mismatch of coefficient of thermal expansion in Al and Si phases.

Even if the mechanisms at work are still hypothetic and must be further investigated, these results could be exploited to propose a new step in the processing route of chip boxes, in view of a lightening of the components thanks to higher mechanical properties. A suitable heat treatment has to be optimized by investigating the effects of heat treatment prior to or in place of temperature cycles.

Declarations of interest

None.

References

Adolfi, S., Jacobson, D.M., Ogilvy, A., "Property Measurements on Osprey Spray-Deposited Al–Si Alloys," Tech. Rep., pp. 1–14, 2002.
Andreasen, J.H., 1994. Reliability-based design of ceramics. Mater. Des. 15 (1), 3–13.

Balzar, D., May–June 1993. X-ray diffraction line broadening: modeling and applications to high-Tc superconductors. J. Res. Natl. Inst. Stand. Technol. 98 (3), 321–353. https://doi.org/10.6028/jres.098.026.

Bristowe, P.D., 1998. Microscopic modelling of grain boundaries and stacking faults in C–Si. Properties of Crystalline Silicon. pp. 299–308.

Chowdhury, P., Sarkar, A., Mukherjee, P., Gayathri, N., Bhattacharya, M., Barat, P., 2010. Studies of microstructural imperfections of powdered Zirconium-based alloys. Mater. Char. 61, 1061–1065. https://doi.org/10.1016/j.matchar.2010.06.019.

Coombs, J., Dunstan, G., "Atomizing Apparatus and Process Part 1," 1993.

Cui, C., Schulz, A., Schimanski, K., Zoch, H.-W., Jun. 2009. Spray forming of hyper-eutectic Al–Si alloys. J. Mater. Process. Technol. 209 (11), 5220–5228.

Davis, J.R. (Ed.), 1993. ASM Specialty Handbook: Aluminum and Aluminum Alloys. ASM International ISBN: 978-0-87170-496-2.

Degen, T., Sadki, M., Bron, E., König, U., Nénert, G., 2014. The High Score suite. Powder Diffraction 29 (4 S2), S13–S18. https://doi.org/10.1017/S0885715614000840.

Del Castillo, L., Hoffman, J.P., Birur, G., Thrivikraman, T., Miller, J., Knowles, T.R., 2013. Robust, reworkable thermal electronic packaging: applications in high power TR modules for space. In: Proceedings of the Aerospace Conference.

Ghassemali, E., Tan, M.-J., Wah, C.B., Lim, S.C.V., Jarfors, A.E.W., 2015. Effect of cold-work on the Hall–Petch breakdown in copper based micro-components. Mech. Mater. 80 (Part A), 124–135. https://doi.org/10.1016/j.mechmat.2014.10.003. January.

Godet, J., 2004. Etude par Simulations et calculs Atomistiques, de la Formation de Dislocations aux Défauts de Surface Dans un Cristal de Silicium Soumis à des Contrainte. Université de Poitiers.

Hildebrandt, W.H., August 1979. Differential scanning calorimetry of recrystallization behavior in aluminum sheet. Metall. Trans. A 10 (8), 1045–1048. https://doi.org/10.1007/BF02811650.

Hirsch, P.B., Roberts, S.G., 1991. The brittle-ductile transition in silicon. Philos. Mag. A 64 (1), 55–80. https://doi.org/10.1080/01418619108206126.

Hogg, S.C., Lambourne, A., Ogilvy, A., Grant, P.S., Jul. 2006. Microstructural characterisation of spray formed Si–30Al for thermal management applications. Scr. Mater. 55 (1), 111–114.

Huang, Y., Humphreys, F.J., May 1999. Measurements of grain boundary mobility during recrystallization of a single-phase aluminium alloy. Acta Mater. 47 (7), 2259–2268. https://doi.org/10.1016/S1359-6454(99)00062-2.

Jia, Y., Cao, F., Scudino, S., Ma, P., Li, H., Yu, L., Eckert, J., Sun, J., 2014. Microstructure and thermal expansion behavior of spray-deposited Al–50Si. Mater. Des. 57, 585–591.

Jones, F.W., 1938. The measurement of the particle size by the X-ray method. Proc. R. Soc. London 166 (924), 16–43.

Kapoor, K., Lahiri, D., Rao, S., Sanyal, T., Kashyap, B., 2004. X-ray diffraction line profile analysis for defect study in Zr-2.5% Nb material. Bull. Mater. Sci. 27, 59–67. https://doi.org/10.1007/BF02708487.

Kohyama, M., Yamamoto, R., Doyama, M., 1986. Reconstructed structures of symmetrical <011> tilt grain boundaries in silicon. Phys. Status Solidi 138, 387–397.

Macherauch, E., Muller, P., 1961. Das sin2ψ-verfahren der röntgenographischen span-nungsmessung. Physik 13, 305–312.

Makhlouf, T., Rebhi, A., Couzinié, J.-P., Champion, Y., Njah, N., Nov 2012. Microstructural evolution of a recycled aluminum alloy deformed by equal channel angular pressing process. Int. J. Miner. Metall. Mater. 19 (11), 1016. https://doi.org/10.1007/s12613-012-0663-6.

Mauduit, D., Dusserre, G., Cutard, T., 2016. Probabilistic rupture analysis of a brittle spray deposited Si–Al alloy under thermal gradient: characterization and thermo-elastic sizing guidelines. Mater. Des. 95, 414–421.

McQueen, H.J., Hockett, J.E., 1970. Microstructures of aluminum compressed at various rates and temperatures. Metall. Trans. 1 (11), 2997–3004. https://doi.org/10.1007/BF03038412.

Mohtadi-Bonab, M.A., Eskandari, M., Szpunar, J.A., 2015. Texture, local misorientation, grain boundary and recrystallization fraction in pipeline steels related to hydrogen induced cracking. Mater. Sci. Eng. A 620, 97–106. https://doi.org/10.1016/j.msea.2014.10.009. 3.

Nohut, S., 2014. Influence of sample size on strength distribution of advanced ceramics. Ceram. Int. 40 (3), 4285–4295. https://doi.org/10.1016/j.ceramint.2013.08.093.

Pelleg, J., Elish, E., Mogilyanski, D., 2005. Evaluation of average domain size and microstrain in a silicide film by the Williamson–Hall method. Metall. Mater. Trans. A 36 (11), 3187–3194.

Perryman, E.C.W., 1954. Observations on the structural changes accompanying recovery in super-purity aluminium. Acta Metall. 2 (1), 26–37. https://doi.org/10.1016/0001-6160(54)90091-7.

Petch, N.J., 1953. The cleavage strength of polycrystals. J. Iron Steel Inst. Lond. 173, 25–28.

Phillpot, S.R., Wolf, D., 1990. Grain Boundaries in silicon from zero temperature through melting. J. Am. Ceram. Soc. 73 (4), 933–937. https://doi.org/10.1111/j.1151-2916.1990.tb05139.x.

Priester, L., 2006. Les Joints De Grains - de La Théorie à L'ingénierie. EDP Sciences In french.

Przybilla, C., Fernández-Canteli, A., Castillo, E., 2013. Maximum likelihood estimation for the three-parameter Weibull cdf of strength in presence of concurrent flaw popula-tions. J. Eur. Ceram. Soc. 33 (Sep. (10)), 1721–1727.

Raju, K., Ojha, S.N., 2014. Effect of spray forming on the microstructure and wear properties of Al–Si alloys. Procedia Mater. Sci. 5, 345–354.

Rebhi, A., Makhlouf, T., Couzinié, J.-P., Champion, Y., Njah, N., 2011. TEM and DSC investigation of the recovery of a recycled aluminum processed by equal channel angular extrusion. Mater. Sci. Forum 667–669, 451–456. https://doi.org/10.4028/www.scientific.net/MSF.667-669.451.

Savage, T.S., Xu, P., Marks, L.D., 1993. Thermal shock cleavage of silicon (111) thin crystals. J. Appl. Phys. 73 (3), 1039–1042. https://doi.org/10.1063/1.353321.

Scardi, P., Leoni, M., Delhez, R., 2004. Line broadening analysis using integral breadth methods: a critical review. J. Appl. Cryst. 37, 381–390. https://doi.org/10.1107/S0021889804004583.

Stokes, A.R., Wilson, A.J.C., 1943. The diffraction of X rays by distorted crystal ag-gregates-I. Proc. Phys. Soc. 56 (3), 174–181.

Trustrum, K., Jayatilaka, 1977. Statistical approach to brittle fracture. J. Mater. Sci. 12, 1426–1430.

Uday, M.B., Ahmad-Fauzi, M.N., Noor, Alias Mohd, Rajoo, S., 2015. An insight into mi-crostructural evolution during plastic deformation in AA6061 alloy after friction welding with alumina-YSZ composite. Mech. Mater. 91, 50–63. https://doi.org/10.1016/j.mechmat.2015.07.010.

Wang, F., Liu, H., Ma, Y., Jin, Y., Apr. 2004. Effect of Si content on the dry sliding wear properties of spray-deposited Al–Si alloy. Mater. Des. 25 (2), 163–166.

Wei, Y., Xiong, B., Zhang, Y., Liu, H., Wang, F., Zhu, B., 2007. Property measurements on spray formed Si–Al alloys. Trans. Nonferrous Met. Soc. China (703), 368–372.

Wei, Y., Xiong, B., Zhang, Y., Liu, H., Wang, F., Zhu, B., 2007. Effect of P/M value on the preforms and microstructures of spray formed 70Si30Al alloy. J. Univ. Sci. Technol. Beijing 14, 141.

Weibull, W., 1951. A statistical distribution function of wide applicability. J. Appl. Mech. 18, 293–297.

Weinshanker, S., Ogilvy, A., Cutter, D., De Lea, R.J., March 2004. High performance, lightweight, hermetic AlSi Packages for military, aerospace, and space applications current packaging technology initial trials. In: Proceedings of the 2nd Advanced Technology Workshop on Military, Aerospace, Space and Homeland Security: Packaging Issues and Applications. Baltimore USA. 28–30.

Williamson, G.K., Hall, W.H., 1953. X-ray line broadening from filed aluminium and wolfram. Acta Metall. 1 (1), 22–31.

Williamson, G.K., Smallman III, R.E., 1956. Dislocation densities in some annealed and cold-worked metals from measurements on the X-ray Debye–Scherrer spectrum. Philos. Mag. J. Theor. Exp. Appl. Phys. 1 (1), 34–46. https://doi.org/10.1080/14786435608238074.

Wu, D., Zhou, J., Li, Y., Jun. 2006. Methods for estimating Weibull parameters for brittle materials. J. Mater. Sci. 41 (17), 5630–5638.

Yu, K., Li, S., Chen, L., Zhao, W., Li, P., Jun. 2012. Microstructure characterization and thermal properties of hypereutectic Si–Al alloy for electronic packaging applications. Trans. Nonferrous Met. Soc. China 22 (6), 1412–1417.

Zhai, W., Zhang, Z., Wang, F., Shen, X., Lee, S., Wang, L., Apr. 2014. Effect of Si content on microstructure and properties of Si/Al composites. Trans. Nonferrous Met. Soc. China 24 (4), 982–988.

Zhao, L.Z., Zhao, M.J., Song, L.J., Mazumder, J., Apr. 2014. Ultra-fine Al–Si hypereutectic alloy fabricated by direct metal deposition. Mater. Des. 56, 542–548.